



HAL
open science

Scalable morphological accessibility of complex microstructures

Johan Chaniot, Maxime Moreaud, Loïc Sorbier, Jean-Marie Becker, Thierry Fournel

► **To cite this version:**

Johan Chaniot, Maxime Moreaud, Loïc Sorbier, Jean-Marie Becker, Thierry Fournel. Scalable morphological accessibility of complex microstructures: (Before review). 2021. hal-03543639v1

HAL Id: hal-03543639

<https://hal.science/hal-03543639v1>

Preprint submitted on 22 Jun 2021 (v1), last revised 26 Jan 2022 (v4)

HAL is a multi-disciplinary open access archive for the deposit and dissemination of scientific research documents, whether they are published or not. The documents may come from teaching and research institutions in France or abroad, or from public or private research centers.

L'archive ouverte pluridisciplinaire **HAL**, est destinée au dépôt et à la diffusion de documents scientifiques de niveau recherche, publiés ou non, émanant des établissements d'enseignement et de recherche français ou étrangers, des laboratoires publics ou privés.

Scalable morphological accessibility of complex microstructures

J., CHANIOT^{1,2}, M., MOREAUD^{1,3}, L. SORBIER¹, J.-M., BECKER², T., FOURNEL²

¹ IFP Energies nouvelles, Rond-point de l'échangeur de Solaize, BP 3, 69360 Solaize, France

² Univ. Lyon, UJM-Saint-Etienne, CNRS, Institute of Optics Graduate School,
Laboratoire Hubert Curien UMR5516, F-42023 St-Etienne, France

³ MINES ParisTech, PSL-Research University, CMM, 35 rue Saint Honoré, 77305 Fontainebleau, France

Abstract

This paper addresses the characterization of dense 3D microstructures using the unifying concept of accessibility, mixing local shape features with global topology. Underlying percolation and constrictivity features are jointly considered by probing the connected components of the microstructure with structuring elements with increasing size. Adapted morphological operations are combined to provide a scalable protocol embedding suitable descriptors applied on accessible volumes, yielding a sharp discrimination power. The suggested framework named A-protocol can efficiently analyze complex microstructures by applying a stratified sampling for the selection of paths' endpoints, when connected. It stops when percolation ends, at a critical radius value. The A-protocol is tested on Cox multi-scale Boolean models using the Euler number as descriptor.

1 Introduction

The analysis of complex patterns or shapes has to combine local -morphological- and global -topological- features [34, 50]. Connectivity, considered under different viewpoints, is of paramount interest in such analyses [40, 51, 15]. Among them, the analysis of artificial or real networks [37, 3] is among the most challenging ones [9].

The structural characterization of 3D microstructures of materials, i.e. interconnected networks, enables valuable connections with physicochemical properties, especially in the analysis of porous media [17, 1]. The concept of accessibility turned out to have a central interest on various experiments making use of different flowing particles and measurement means [46, 16, 30, 42]. Hindrance in porous media is indeed crucial as the size of flowing particles can impact transport properties, especially when it has the same order of magnitude as the pores dimensions [49, 43]. In the digital domain, after microstructure segmen-

tation, hindrance could be addressed in the scope of morphological accessibility, defined here by combining connectivity seen through percolation, i.e. ability to connect, with constrictivity, i.e. the strength of bottleneck effect [10]. Throughout the article, the term "accessibility" will mean "morphological accessibility". Percolation as a theory considers accessibility in a specific way [8, 45, 18], indicating the existence of a connected path totally included in the pattern, connecting a given entry to a given exit, thus linked to global topological notions (Fig.1(A-D)). The numerical implementations of percolation are of distinct types [39]. Constrictivity [32] highlights local hindrance through bottleneck effects quantification, usually represented by a scalar value named constriction factor. Originally defined for a synthetic pore (Fig.1(e)), extensions to microstructures exist [20, 29].

One can find similar ideas based on morphological operations, taking into account the local shape in order to address accessibility, reachability or penetrability [48, 47, 31, 10]. Mor-

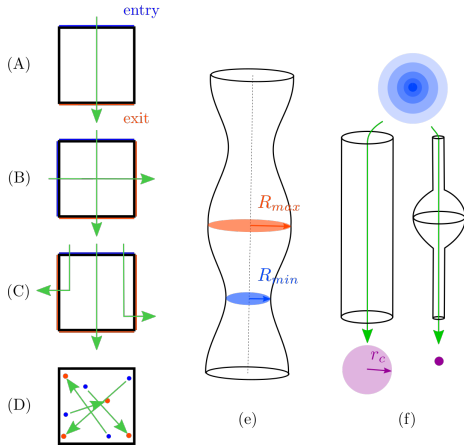


Figure 1: (A-D) Four forms of percolation: (A) directional percolation (between two opposite faces), (B) multi-directional percolation (in at least one direction), (C) adirectional percolation (between distinct faces) [12], and (D) stochastic percolation [11] (between random points). Illustration of (e) constrictivity and (f) accessibility with critical radius r_c (see Section 2).

phological opening or erosion, by spheres with variable radius [41, 44], computed using distance transform [36, 7], are utilized for characterization purposes according to pores' or particles' size, quantifying disconnections. Erosion is more adapted to topological measurements, while opening is suitable for geometric ones. Connectivity between parallel planes is then computed using either connectivity functions based on the Euler number [48, 47], or percolation probability [31] or statistical percolation [10]. The percolation is assessed utilizing a connected components labeling, assigning a specific label to each connected component [19, 35]. In order to remove the constraint of choosing planar sections as entries and exits, [11, 13] make use of a stratified sampling [4], yielding to a stochastic consideration of percolation, assessed between random points or vertices, in a certain way akin to graph theory [27]. Spherical probes of different sizes travelling through the network could be a common basis for accessibility, as illustrated in Fig.1(f).

The main contribution of this article is a scalable framework able to support the different forms of percolation illustrated in Fig.1(A-D), and jointly constrictivity illustrated in Fig.1(e). The computational protocol proposed in Section 2, named *A-protocol*, provides a versatile methodology addressing accessibility via 3D patterns. It is suitable for any specific application-dependent descriptors, extending it in an easily interpretable manner, as shown below with the Euler number. Its effectiveness is tested on Cox multi-scale Boolean models, focusing on the stochastic form of percolation and accessibility, in order to assess its potentiality in terms of discriminative power: the results quantifying local anisotropy and global heterogeneity are reported in Section 3. The conclusion is drawn in Section 4.

2 The *A-protocol*

The *A-protocol* is an iterative method taking into account all bottlenecks of a microstructure by considering increasing radii r for sphere $B(r)$ used as structuring element for morphological erosions. At each iteration, percolation is jointly verified after labeling connected components, and predefined embedded descriptors are assessed. Some *cavities* defined as the resulting non-accessible connected components for a probe of a given size, are formed due to the hindrance caused by the probe dilation. Geometrically, the larger the radius, the more there will be vanished volumes. Topologically, the trajectories between any two remaining points of the microstructure, lengthen until they are closed. The focus being mainly on topological measurements and computation time efficiency, the erosion operation was chosen and S defined once for all at the initialization step. As the *A-protocol* is a cumulative step by step process, if residues descriptors are considered, as cavities, the value of the descriptor for a specific size is equal to the sum over these residues from $r = 0$ to the given size. The *A-protocol* ends when the *critical radius* r_c i.e. the radius of the biggest percolating spherical probe $B(r_c)$,

is reached. Sampling 3D patterns is optional but required in the context of stochastic percolation giving rise to *stochastic accessibility*, that we define herebelow,

Definition 1. Stochastic accessibility: Let $\epsilon_r(X)$ be the eroded set of microstructure X using a sphere $B(r)$ as structuring element. Let $S = \{p_i\}$ be a set of N random points such that $S \subset \epsilon_r(X)$. A connected component of $\epsilon_r(X)$ is said to percolate if at least a number θ of connected paths exists between some pairs of points, (p_i, p_j) , $i \neq j$. Eroded set $\epsilon_r(X)$ percolates if there exists at least a percolating connected component.

Let Cc_r be the union of the percolating connected components of $\epsilon_r(X)$. If $Cc_r \neq \emptyset$, X is said to be accessible for a probe $B(r)$.

In order to comply with usual definitions, we take $\theta = 1$; for a connected component to be considered as *accessible*, it suffices that a connected path has been found. The *stochastic accessibility* allows the *A-protocol* to be applied on any microstructures, reflecting the flowing particles in the physical domain.

The definition of a protocol devoted to accessibility is motivated by the transfer of the concept into a scalable digital framework embedding relevant descriptors, with efficiency concerns. The *A-protocol* illustrated in Fig.2 on a synthetic structure, is formally given by the algorithm below. The estimates of accessible volume fraction \hat{V}_{v_A} , number of cavities \hat{N}_C , and average volume of cavities \hat{V}_C are simultaneously assessed until the *critical radius* \hat{r}_c is reached. Let us note that the skeleton of microstructure X [38, 21] could be considered, but would lead to increase the bias over morphological descriptors as volume fraction assessments.

3 Results

For testing the *A-protocol* and illustrating its properties on complex microstructures, stochastic models so numerical twins are considered, focusing on *stochastic accessibility*. For

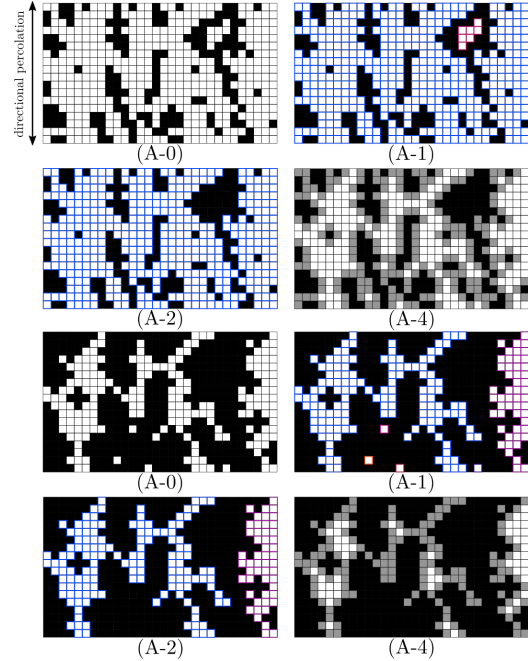


Figure 2: Analysis of a synthetic structure (in white) by the *A-protocol*; directional percolation and $\hat{r}_c = 1$. (A-0) shows the pattern state at the starting of an iteration, (A-1) connected components labeling, each label being associated with a color, (A-2) percolation assessment with deletion of non percolating connected components, (A-3) (not displayed) computation of descriptors, (A-4) morphological erosion using $B(1)$, deleted pixels being in gray.

Input: Pattern X ; embedded descriptor $\{D_k\}$; (optional) sampling point set S

Output: Estimates $\hat{V}_{v_A}, \hat{N}_C, \hat{V}_C$ and embedded descriptor $\{\hat{D}_k\}$, as functions of r ; *critical radius* \hat{r}_c

Initialization: $r \leftarrow 0$

while *Percolation* **do**

A-1. Connected components labeling
 $X \leftarrow \{cc_i\}$ (Fig.2(1))

A-2. Percolation assessment and computation of Cc_r (Fig.2(2))

if *Percolation* **then**

A-3. Computation of estimates $\hat{V}_{v_A}(r), \hat{N}_C(r), \hat{V}_C(r)$ and embedded descriptor $D_k(r)$ over Cc_r

A-4. Erosion, $X \leftarrow \epsilon_1(X)$ (Fig.2(4))

Incrementation: $r \leftarrow r + 1$

end

end

Critical radius: $\hat{r}_c \leftarrow r - 1$

Algorithm 1: *A-protocol*

this purpose, Cox multi-scale Boolean models which are suitable for both theoretical and statistical analyses of computational methods and usual investigation of stereological operators [2] are used. First, theoretical relationships connecting the *critical radius* to constrictivity and percolation are given. Second, the *A-protocol's* behavior analysis with respect to specific features is practicable; impact of the grains' anisotropy and the geometric heterogeneity over the accessibility to the microstructure.

3.1 Cox multi-scale Boolean models

Boolean models [24, 14] are considered in order to generate homogeneous microstructures made of anisotropic grains A' , located at Poisson points. Hereafter, they are defined by a single volume fraction of grains V_v . Multi-scale microstructures can be modeled by using Cox multi-scale Boolean models [22, 26], simulating heterogeneous materials. In the following, two-scale models are considered, defined by three volume fractions: $V_{v,INC}$ for aggregates with higher density, V_v for grains inside aggregates, and $V_{v,OUT}$ for grains outside aggregates. Boolean models of spheres (Fig.3(a)) and of spherocylinders with random orientations (Fig.3(b)) are generated; $V_v = 0.4$ for both models, having similar average volume of grain, $\bar{V}(A') = 4188.8$ for spheres and $\bar{V}(A') = 4215.0$ for spherocylinders.

1. sphere $R = 10$,
2. spherocylinder $R = 5$ and $L = 47$.

Cox multi-scale Boolean models of platelets are considered; platelets' shape (Fig.3(c)): $L = 6$, $l = 5$ and $h = 3$, and aggregates' size and volume fraction: $R_{INC} = 10$, $V_{v,INC} = 0.5$, are fixed.

3. $V_v = 0.5$ and $V_{v,OUT} = 0.3$,
4. $V_v = 0.6$ and $V_{v,OUT} = 0.2$,
5. $V_v = 0.7$ and $V_{v,OUT} = 0.1$.

40 realizations of size 400^3 of each model are generated (Fig.3). The *A-protocol* is applied to the complementary set of the grains union (black areas in Fig.3). Confidence intervals with 95 % confidence level, represented by vertical bars in the results display, are equal to $2l_\sigma$, with $l_\sigma = 2\sigma/\sqrt{n_r}$, and σ the standard deviation over the n_r realizations. Finally, in this case, the *A-protocol* provides averaged assessments; let π be a given descriptor, then $\hat{\pi}$ is an averaged estimator over all realizations.

3.2 *A-protocol*: discussions

Constrictivity factors β quantifying bottlenecks, are scalar values obtained from comparison of minimal and maximal cross sections [20, 6]. A specific definition consists in computing the squared ratio of the minimal to the maximal radius, which could be translated in our case by using the *critical radius* r_c and the maximal radius, i.e. the maximal distance value D_{max} obtained from the distance map used for the iterative erosions.

$$\beta = \left(\frac{r_c}{D_{max}} \right)^2 \quad (1)$$

By definition the *critical radius* r_c is linked to the critical percolation threshold ρ_c , which can be assessed using a statistical approach [23], then defined as the volume fraction where exactly 50% of the realizations percolate. Considering Boolean models, the density θ of grains A' is given by:

$$1 - V_v = \exp(-\theta \cdot \bar{V}(A')) \quad (2)$$

with V_v the volume fraction of grains of the model A , and $\bar{V}(A')$ the average volume of grains A' . Let $A_r = A \oplus B(r)$ be a Boolean model defined as the dilation of A by $B(r)$, and $V_{v,r}$ be the volume fraction of A_r . As $V_{v,r} \geq V_v$, there exists a function α , $\forall r \geq 1 \alpha(r) \geq 1$, such that $\bar{V}(A'_r) = \alpha(r) \cdot \bar{V}(A')$. Therefore, with eq.2, $1 - V_{v,r} = (1 - V_v)^{\alpha(r)}$.

Henceforth, r_c is a limit value of r , obtained when $1 - V_{v,r}$ is equal to the threshold ρ_c of the eroded complementary set. Therefore, there

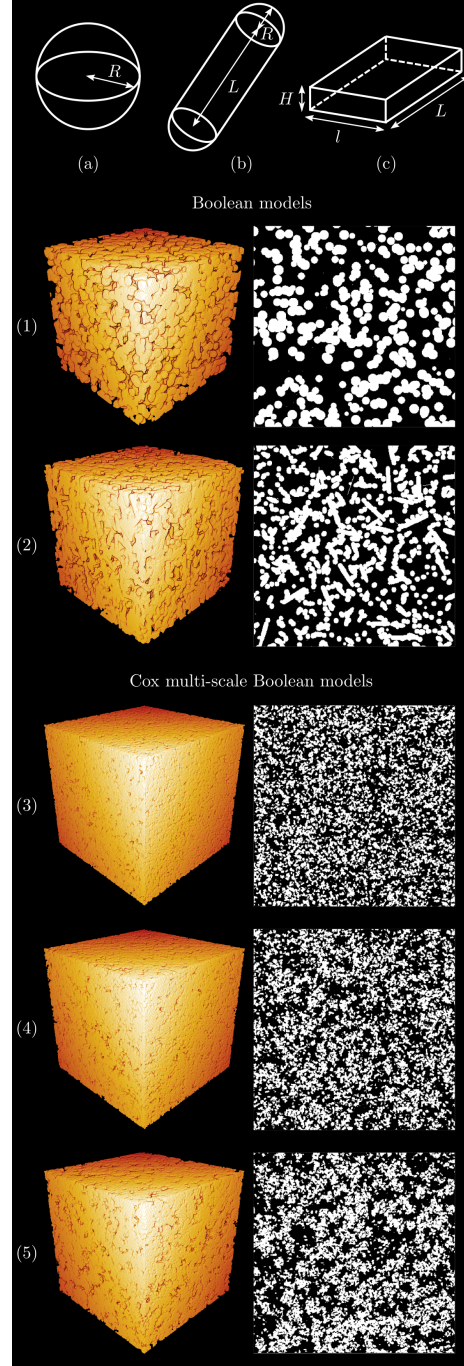


Figure 3: The different grain's shapes used in this paper: (a) sphere, (b) spherocylinder and (c) platelet. Volume representation and 2D slice of a realization of each Boolean model: (1) spheres and (2) spherocylinders, and Cox multi-scale Boolean models of platelets: (3) $V_v = 0.5$, (4) $V_v = 0.6$ and (5) $V_v = 0.7$. Volumes generated and rendered using [33].

exists $\alpha_c = \alpha(r_c)$ and,

$$\alpha_c = \ln(\rho_c) / \ln(1 - V_v). \quad (3)$$

If $A' = B(R)$, therefore $\alpha_c = ((R + r_c) / R)^3$ and,

$$r_c = \left(\sqrt[3]{\ln(\rho_c) / \ln(1 - V_v)} - 1 \right) .R. \quad (4)$$

Considering Cox multi-scale Boolean models, the total volume fraction of primary grains $V_{v,TOT}$ is defined by,

$$V_{v,TOT} = V_{v,INC} . V_v + (1 - V_{v,INC}) . V_{v,OUT}. \quad (5)$$

Eq.2 is valid for each volume fraction and the same rationale leads to,

$$\rho_c = (1 - V_v)^{\alpha_c} - (1 - V_{v,INC}) . ((1 - V_v)^{\alpha_c} - (1 - V_{v,OUT})^{\alpha_c}). \quad (6)$$

Let us now restrict our attention to the model (1). Only \hat{r}_c and \hat{V}_{v_A} are displayed in Tab.1 and Fig.4. As a global statement, the low values of l_σ attest the representativity of the considered volume, i.e. the realizations' volume times the realizations number. Confidence intervals of all curves are represented, but too small to be visible before a certain value; the larger the radius r , the bigger the representative volume element, the lower the representativity [28].

The stratified sampling is a parametric method, with N_T and N the target number given by the user and the final number of random points, respectively [11]. None of them is meaningful, but the length of the cubic sub-images' edges e is. The purpose is to assess its optimal value with respect to an arbitrary reference, the percolation (A) ($\hat{r}_{c,ref}$, $\hat{V}_{v_{A,ref}}$). The *A-protocol* with *stochastic accessibility*, is analyzed as a function of $e = \{133, 100, 80, 66\}$ (Fig.4(a)). One can notice some slight differences with (A) due to negligible volumes (Fig.4 bottom right); Fig.4(a) shows the similarities of \hat{V}_{v_A} whatever e . The best assessment of ($\hat{r}_{c,ref}$, $\hat{V}_{v_{A,ref}}$) is reached for $e = 100$ ($N = 64$). The same process is performed on each model showing a necessary refinement for the more complex

Table 1: 1st line: \hat{r}_c for the stochastic accessibility with different e values. 2nd line: \hat{r}_c for the various accessibility types. Display of l_σ , the half length of the confidence interval, with 95 % confidence level.

Model	Percolation	\hat{r}_c	l_σ
(1) Sphere	Stochastic $e = 133$	9.175	0.311
	Stochastic $e = 100$	9.05	0.237
	Stochastic $e = 80$	9.4	0.266
	Stochastic $e = 66$	10.95	0.531
(1) Sphere	A	8.9	0.096
	B	8.975	0.05
	C	13.95	0.423
	D	9.05	0.237

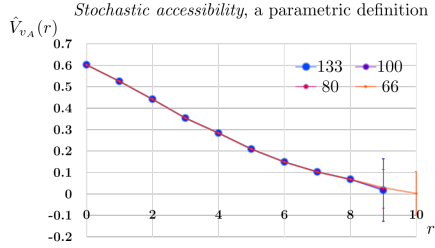
ones; (1) $e = 100$, (2) $e = 100$, and (3) $e = 100$, (4) $e = 80$ ($N = 125$), (5) $e = 80$. Hereafter, these values are considered in percolation (D).

Let us compare now the four percolation forms (Fig.4(b)). Globally, the curves are quite similar whatever the percolation. The considered models being isotropic, the percolations (A) and (B) exhibit very similar results, as for the percolation (D). The accessible volume in Fig.4 bottom, places in evidence the similarities and differences; in particular (C), as less constrained, overestimates (A), but the low representativity of the remaining connected components is shown.

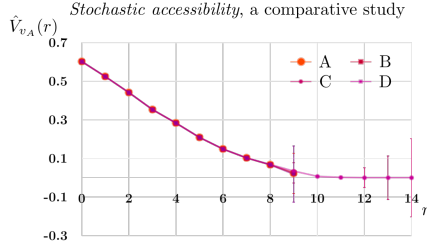
3.3 Microstructures characterization

The focus is now on the *A-protocol* with *stochastic accessibility* only. Although \hat{r}_c is sufficient to discriminate the models in Tab.2, additional information is provided by the behavior of the estimates and the Euler number χ ; the more negative χ , the more interconnected the microstructure.

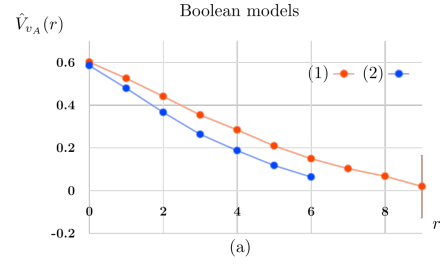
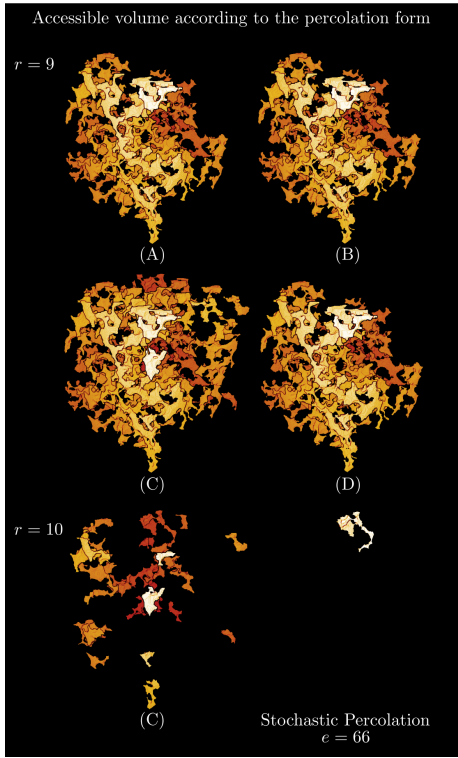
The anisotropy of the spherocylinder, characterized by its morphological diameter too, strongly induces the creation of cavities when r increases; the more pronounced the bottleneck effects, the faster the pores' closing, the faster



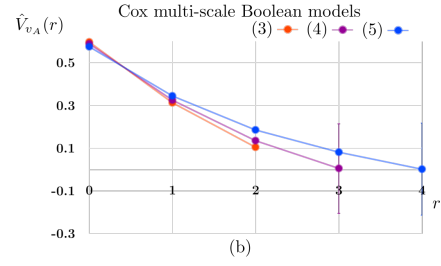
(a)



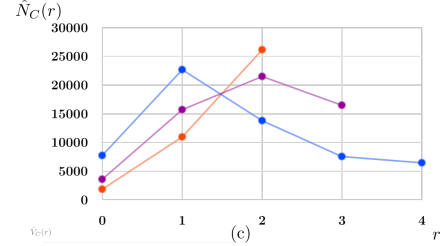
(b)



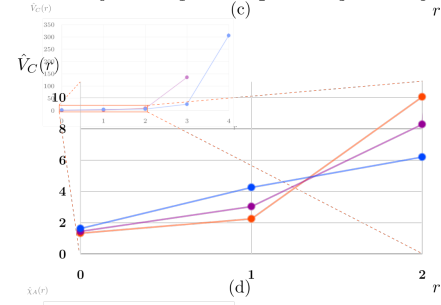
(a)



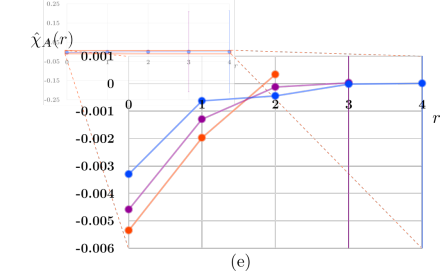
(b)



(c)



(d)



(e)

Figure 4: \hat{V}_{v_A} for (a) the stochastic percolation ($e \in \{133, 100, 80, 66\}$) and (b) the four forms of percolation ((A), (B), (C), (D)), applied to Boolean models (1). Confidence intervals, with 95 % confidence level, are represented by vertical bars. The accessible volume of a realization of the Boolean model (1) for specific radii: $r = 9 = \hat{r}_{c,ref}$ and $r = 10$. Volumes rendered using [33].

Figure 5: A-protocol with stochastic accessibility applied to the Boolean models (a) \hat{V}_{v_A} , and Cox multi-scale Boolean models: (b-d) A-protocol estimates and (e) $\hat{\chi}_A$ ((d-e) are enlargements, orange rectangle, of original curves, small and blurred). Confidence intervals, with 95 % confidence level, are represented by vertical bars.

Table 2: \hat{r}_c for the stochastic accessibility with optimal e values, for all models. Display of l_σ , the half length of the confidence interval, with 95 % confidence level.

Model	\hat{r}_c	l_σ
(1) Sphere	9.05	0.237
(2) Spherocylinder	6.325	0.166
(3) $V_v = 0.5$	2	0
(4) $V_v = 0.6$	2.575	0.158
(5) $V_v = 0.7$	3.575	0.174

the decrease of accessible volume. Fig.5(a) displays the decrease of accessibility with the grains' anisotropy. Considering the models (3-5), χ is assessed as a function of the probe's radius; its extension and numerical estimator are named χ_A and $\hat{\chi}_A$, respectively. Fig.5(b-e) underlines the good discrimination between the distinct heterogeneities, naturally involving cavities formation; for $V_{v,TOT}$ fixed and $V_{v,INC} = 0.5$, globally, the more heterogeneous the microstructure, the less dense the exterior of aggregates, the slower the porous network closes because of the enlarging of the pores size, decreasing the strength of bottleneck effects. This second case attests to the increase of accessibility with heterogeneity for large enough particles. Furthermore, it highlights the improvement of the sensitivity of the extended descriptor, the Euler number. At a finer scale, the *A-protocol* puts in evidence the classification reversal of topological measures \hat{N}_C , \hat{V}_C and $\hat{\chi}_A$, attesting of the heterogeneity of these models (Fig.5(b-d)). Indeed, this behavior, corresponding to the very "moment" of the aggregates closing, provides models' discrimination; in particular between homogeneous (models (1-2)) and heterogeneous materials (models (3-5)). Consequently, together, these cases bring novel information about heterogeneity detection. The computations have been performed for the five models, supporting these conclusions.

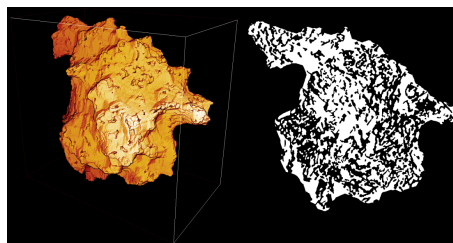


Figure 6: A sample of a specific γ -alumina, obtained by electron tomography, reconstructed, filtered, and segmented: (left) the porous volume, (right) a slice. Volumes rendered using [33].

4 Conclusion

The *A-protocol* combines state-of-the-art definitions dynamically considering the accessibility, aiming to extend any given numerical descriptor definition with topological notions. The *A-protocol* integrates all bottleneck effects, detected by the spherical probe with increasing radii, and gives rise at the end to estimates as the *critical radius*. The *A-protocol* is illustrated using Cox multi-scale Boolean models, validating its interest as a new "extractor" of morphological and topological information. The *A-protocol* with the *stochastic accessibility*, providing a less restrictive method through the existence of a connected path between random points, is discussed. This analysis attests the similarities of this definition with the most common definition in the literature, yielding a good estimator. The Euler number is then considered, illustrating together with the estimates, the enhancement of discriminative power when characterizing multi-scale microstructures; anisotropy discrimination and heterogeneity detection and discrimination. The *A-protocol* exacerbating initially imperceptible differences, is able to characterize microstructures whatever their complexity, inherent to the materials and/or stemming from the image acquisition device, thanks to the *stochastic accessibility*. Consequently, real materials as the γ -alumina (Fig.6), can be characterized with any morphological descriptors, extending the work of [25] and opening wide application

perspectives. Also, a deterministic extension of the *A-protocol* will be defined, similarly to [5]. Finally, a grayscale extension would allow the consideration of continuous fields [47]. The *A-protocol* procedure is available in the open access software environment *plug im!* [33].

References

- [1] P.M. Adler and J.-F. Thovert. "Real porous media: Local geometry and macroscopic properties". In: *Applied Mechanics Reviews* 51.9 (1998), pp. 537–585.
- [2] A. Aubert and D. Jeulin. "Estimation of the influence of second- and third-order moments on random sets reconstructions". In: *Pattern Recognition* 33.6 (2000), pp. 1083–1104.
- [3] A.R. Backes and O.M. Bruno. "Shape classification using complex network and multi-scale fractal dimension". In: *Pattern Recognition Letters* 31.1 (2010), pp. 44–51.
- [4] A. Baddeley and E.B.V. Jensen. *Stereology for statisticians*. Chapman and Hall/CRC, 2004.
- [5] A.T.F. Batista et al. "Atomic Scale Insight into the Formation, Size, and Location of Platinum Nanoparticles Supported on γ -Alumina". In: *ACS Catalysis* 10.7 (2020), pp. 4193–4204.
- [6] F. Bini et al. "A 3D Model of the Effect of Tortuosity and Constrictivity on the Diffusion in Mineralized Collagen Fibril". In: *Scientific reports* 9.1 (2019), p. 2658.
- [7] G. Borgefors. "Distance transformations in digital images". In: *Computer Vision, Graphics, and Image Processing* 34.3 (1986), pp. 344–371.
- [8] S.R. Broadbent and J.M. Hammersley. "Percolation processes: I. Crystals and mazes". In: *Mathematical Proceedings of the Cambridge Philosophical Society*. Vol. 53. 3. Cambridge University Press. 1957, pp. 629–641.
- [9] D. Bujoreanu et al. "Robust graph representation of images with underlying structural networks. Application to the classification of vascular networks of mice's colon". In: *Pattern Recognition Letters* 87 (2017), pp. 29–37.
- [10] J. Chaniot et al. "The reachable volume fraction in porous media in the vicinity of percolation threshold: a numerical approach used on multi-scale Boolean schemes". In: *2017 16th Workshop on Information Optics (WIO)*. IEEE. 2017, pp. 1–3.
- [11] J. Chaniot et al. "Tortuosimetric operator for complex porous media characterization". In: *Image Analysis & Stereology* 38.1 (2019), pp. 25–41.
- [12] Johan Chaniot. "Caractérisation morphologique efficace de matériaux par cartes de distance". PhD thesis. University of Lyon, 2019.
- [13] Johan Chaniot et al. "Heterogeneity assessment based on average variations of morphological tortuosity for complex porous structures characterization". In: *Image Analysis & Stereology* 39.2 (2020), pp. 111–128.
- [14] S.N. Chiu et al. *Stochastic geometry and its applications*. John Wiley & Sons, 2013.
- [15] L.N. Couto, A.R. Backes, and C.A.Z. Barcelos. "Texture characterization via deterministic walks' direction histogram applied to a complex network-based image transformation". In: *Pattern Recognition Letters* 97 (2017), pp. 77–83.
- [16] D.D. Do et al. "The role of accessibility in the characterization of porous solids and their adsorption properties". In: *Adsorption* 16.1-2 (2010), pp. 3–15.
- [17] F.A.L. Dullien. *Porous media: fluid transport and pore structure*. Academic Press, 1979.
- [18] C. Gotsman. "A cluster detection algorithm based on percolation theory". In: *Pattern Recognition Letters* 12.4 (1991), pp. 199–202.

- [19] L. He et al. "The connected-component labeling problem: A review of state-of-the-art algorithms". In: *Pattern Recognition* 70 (2017), pp. 25–43.
- [20] L. Holzer et al. "The influence of constrictivity on the effective transport properties of porous layers in electrolysis and fuel cells". In: *Journal of Materials Science* 48.7 (2013), pp. 2934–2952.
- [21] S. Iglesias-Cofán and A. Formella. "Guided thinning". In: *Pattern Recognition Letters* 128 (2019), pp. 176–182.
- [22] D. Jeulin. "Morphology and effective properties of multi-scale random sets: A review". In: *Comptes Rendus Mécanique* 340.4-5 (2012). Recent Advances in Micromechanics of Materials, pp. 219–229.
- [23] D. Jeulin and M. Moreaud. "Percolation of random cylinder aggregates". In: *Image Analysis & Stereology* 26.3 (2007), pp. 121–127.
- [24] G. Matheron. "Random sets and integral geometry". In: *J. Wiley, New York* (1975).
- [25] M. Moreaud, B. Celse, and F. Tihay. "Analysis of the accessibility of macroporous alumino-silicate using 3D-TEM images". In: *Proceedings of Materials Science & Technology 2008 Conference and Exhibition: MS&T*. Vol. 8. 2008, pp. 1153–64.
- [26] M. Moreaud et al. "Multi-scale stochastic morphological models for 3D complex microstructures". In: *2018 17th Workshop on Information Optics (WIO)*. IEEE. 2018, pp. 1–3.
- [27] L. Najman and J. Cousty. "A graph-based mathematical morphology reader". In: *Pattern Recognition Letters* 47 (2014), pp. 3–17.
- [28] M. Neumann et al. "On variability and interdependence of local porosity and local tortuosity in porous materials: a case study for sack paper". In: *Methodology and computing in applied probability* (2020), pp. 1–15.
- [29] Matthias Neumann et al. "Quantifying the influence of microstructure on effective conductivity and permeability: virtual materials testing". In: *International Journal of Solids and Structures* 184 (2020), pp. 211–220.
- [30] N. Nishiyama and T. Yokoyama. "Permeability of porous media: role of the critical pore size". In: *Journal of Geophysical Research: Solid Earth* 122.9 (2017), pp. 6955–6971.
- [31] J. Ohser et al. "Estimation of the probability of finite percolation in porous microstructures from tomographic images". In: *International journal of materials research* 103.2 (2012), pp. 184–191.
- [32] E.E. Petersen. "Diffusion in a pore of varying cross section". In: *AIChE Journal* 4.3 (1958), pp. 343–345.
- [33] plug im! *plug im!: an open access and customizable software for signal and image processing*. 2018. URL: <https://www.plugin.fr>.
- [34] E. Richardson and M. Werman. "Efficient classification using the Euler characteristic". In: *Pattern Recognition Letters* 49 (2014), pp. 99–106.
- [35] F. Diaz-del Rio et al. "Parallel connected-Component-Labeling based on homotopy trees". In: *Pattern Recognition Letters* 131 (2020), pp. 71–78.
- [36] A. Rosenfeld and J.L. Pfaltz. "Distance functions on digital pictures". In: *Pattern Recognition* 1.1 (1968), pp. 33–61.
- [37] D. Rutovitz. "Pattern Recognition". In: *Journal in Royal Statistical Society: Series A* 129.4 (1966), pp. 504–527.
- [38] P.K. Saha, G. Borgefors, and G. S. di Baja. "A survey on skeletonization algorithms and their applications". In: *Pattern Recognition Letters* 76 (2016), pp. 3–12.
- [39] M. Sahimi. *Applications of percolation theory*. CRC Press, 1994.

- [40] P. Saint-Marc, M. Hospital, and M. Richetin. "Pattern recognition by traversal of connected components of a line segments field". In: *Pattern Recognition Letters* 6.3 (1987), pp. 163–168.
- [41] J. Serra. *Image analysis and mathematical morphology*. Academic Press, Inc., 1982.
- [42] Y. She et al. "Accessibility of the pores in highly porous alumina films synthesized via sequential infiltration synthesis". In: *Nanotechnology* 29.49 (2018), p. 495703.
- [43] M.J. Skaug et al. "Hindered nanoparticle diffusion and void accessibility in a three-dimensional porous medium". In: *ACS nano* 9.2 (2015), pp. 2148–2156.
- [44] P. Soille. *Morphological image analysis: principles and applications*. Springer Science & Business Media, 2013.
- [45] D. Stauffer. *Introduction to percolation theory*. Francis & Taylor, 1985.
- [46] F. Thibault-Starzyk et al. "Quantification of enhanced acid site accessibility in hierarchical zeolites—the accessibility index". In: *Journal of Catalysis* 264.1 (2009), pp. 11–14.
- [47] H.-J. Vogel. "Topological characterization of porous media". In: *Morphology of condensed matter*. Springer, 2002, pp. 75–92.
- [48] H.J. Vogel. "Morphological determination of pore connectivity as a function of pore size using serial sections". In: *European Journal of Soil Science* 48.3 (1997), pp. 365–377.
- [49] V. Wernert, R. Bouchet, and R. Denoyel. "Influence of molecule size on its transport properties through a porous medium". In: *Analytical Chemistry* 82.7 (2010), pp. 2668–2679.
- [50] C. Yang et al. "Shape-based object matching using interesting points and high-order graphs". In: *Pattern Recognition Letters* 83 (2016), pp. 251–260.
- [51] Z. Zhou et al. "Exploring generalized shape analysis by topological representations". In: *Pattern Recognition Letters* 87 (2017), pp. 177–185.